TABLE I. Ratio R of the self-polarization to RKKY field for perfectly screened (R_1) and unscreened (R_2) exchange, as a function of $\alpha = 2k_F R_{12}$.

$\alpha = 2k_F R_{12}$	$R_1(\alpha)$	$R_2(\alpha)$
0.4	0.1340	0.1326
0.8	0.1628	0.1543
1.2	0.2160	0.1846
1.6	0.2992	0.2174
2.0	0.4217	0.2564
2.4	0.6052	0.3102
2.8	0.8938	0.3768
3.2	1.3797	0.4388
3.6	2.2915	0.4848
4.0	4.3478	0.5240
4.4	11.2410	0.5716
4.8	−1000.0000	0.6412

R_1 is 1.75. Thus, we see that the self-polarization effect may be quite important and may have a larger contribution than the RKKY term itself.

For the case of Hartree-Fock unscreened exchange, the α dependence of the ratio R_2, is rather slow. For PrBi, the self-polarization field is nearly 46% of the RKKY molecular field. Although its magnitude is smaller than that obtained by using perfectly screened exchange, in both cases, the effect is more important than the short-range correlation effects pointed out by Cooper.[4] This latter correlation was estimated to be of the order of 15–20% of the molecular-field term.

The sensitive dependence of R on the choice of a particular form of exchange integral clearly indicates that one has to be quite careful in any detailed quantitative analysis of the susceptibility and critical-exchange parameter. In conclusion, we would like to emphasize that the self-polarization effect, neglected in calculations until now, is expected to play an important role in the magnetic properties of rare-earth group-V intermetallic compounds with singlet ground states.

ACKNOWLEDGMENTS

We are grateful to Dr. W. F. Brinkman and Dr. Y. Yafet for helpful discussions.

[1]R. J. Elliott, Proc. Phys. Soc. (London) 70, 119 (1957).
[2]G. T. Trammell, J. Appl. Phys. Suppl. 31, 362 (1960).
[3]G. T. Trammell, Phys. Rev. 131, 932 (1963).
[4]B. R. Cooper, Phys. Rev. 163, 444 (1967).
[5]B. Bleaney, Proc. Roy. Soc. (London) 276A, 19 (1963).
[6]M. A. Ruderman and C. Kittel, Phys. Rev. 96, 99 (1954); K. Yosida, *ibid.* 106, 893 (1957).
[7]The idea of self-polarization has been applied in the literature in different contexts, for example, in the Zener theory of ferromagnetism. (Also see Ref. 13 where the coupling between two moments via spin-density waves has been analyzed.) In this paper, the self-polarization effect is being applied in a new context.
[8]T. Kasuya, Progr. Theoret. Phys. (Kyoto) 16, 45 (1956).
[9]R. E. Watson, in *Hyperfine Interactions*, edited by A. J. Freeman and R. B. Frenkel (Academic, N. Y., 1967), p. 437.
[10]R. E. Watson and A. J. Freeman, Phys. Rev. 152, 566 (1966).
[11]K. Andres and E. Bucher, Phys. Rev. Letters 22, 600 (1969).
[12]E. Bucher (private communication).
[13]A. W. Overhauser, J. Appl. Phys. Suppl. 34, 1019 (1963).

PHYSICAL REVIEW B VOLUME 3, NUMBER 1 1 JANUARY 1971

Electron States in Ferromagnetic Iron. I. Band Properties

K. J. Duff* and T. P. Das†
University of California, Riverside, California 92507
(Received 6 April 1970)

A new band-structure calculation is reported for the ferromagnetic state of iron, in which the exchange interaction is given particularly careful treatment. A variational procedure was used with the wave functions expanded in terms of tight-binding functions and orthogonalized plane waves. Hybridization and spin polarization of the wave functions were allowed. Correlation corrections were incorporated. The energy bands are somewhat wider than those previously published; comparison is made with photoemission and optical reflection and x-ray emission data. The calculation leads self-consistently to the observed magnetic moment. The roles of intra-atomic exchange and itinerancy in the origin of iron's ferromagnetism are discussed.

I. INTRODUCTION

It has long been clear from both experimental and theoretical points of view that in the transition metals the conduction electrons consist of semilocalized

$3d$ electrons and very diffuse $4s$-$4p$-··· electrons. If this dichotomy could be applied strictly, the band structures of these elements could be calculated for the $3d$ electrons independently of those for the $4s$-··· electrons. In particular, the simplicity of the tight-binding (TB) method[1] could be exploited for the former, and the orthogonalized-plane-wave (OPW) method[1] would easily apply to the latter. However, hybridization[2] of otherwise overlapping energy bands can occur in some regions of the Brillouin zone (BZ), so the demands placed on the band-structure problem become more severe. The Green's-function and augmented-plane-wave (APW) methods[1] have both been very successful in accommodating the conflicting requirements of compact and diffuse wave functions, and from a single calculation can produce both types of states, fully hybridized where hybridization occurs. Unfortunately, in the present formulation of these approaches, only local potentials can be treated. For the case of iron, the magnetic properties hinge on the nonlocal exchange interaction, and to gain insight into these properties it is desirable to avoid making localizing approximations. The present consideration of iron attempts an accurate treatment of exchange, while satisfying the requirements on the spatial behavior of the wave functions.

In this work attention was restricted to the conduction-electron states, and we will frequently refer to these as $3d$ or $4s$ electrons or as $3d$- or $4s$-like, but it is not intended that this description implies that the wave functions of electrons so described are characteristically atomlike. The method chosen was a variational one in which the components of the wave function have both localized and diffuse character, and full hybridization is allowed at all points at which energies are calculated. The conduction-electron wave functions are allowed to be spin polarized even when they consist mostly of tight-binding d wave functions. For exchange, the exact Hartree-Fock expressions were used and computed as accurately as possible, except where theoretical considerations suggested a screened exchange was more appropriate. Correlation effects are included explicitly through the screened-exchange-Coulomb-hole approximation[3] for $4s$-like states and the effective-exchange-interaction[4] formalism for the d-band states. This treatment of the d-band correlation problem bears some resemblance to a recent pseudopotential calculation for nickel.[5] The computational aspects of this treatment are described in Secs. II–V.

This calculation has been successful in describing many of the static electronic properties of iron. In Secs. VI–IX we describe those properties which are related to the band structure. We defer to a separate paper the discussion of properties related to the electronic wave functions.[6]

II. GUIDING PRINCIPLES

Several band structures for paramagnetic iron[7] have been reported. For these, ferromagnetism is obtained by assuming a $\vec{k}$-independent shift of the minority-spin bands towards higher energies relative to the majority-spin bands. The amount of shift required is adjusted to fit the known magnetic moment. Three band structures have been reported for ferromagnetic iron.[8–11] In each case ferromagnetism is obtained by artificial adjustments of the Slater $\rho^{1/3}$ exchange.

From all of these calculations a few features have emerged as a consistent pattern and they are, therefore, incorporated in the new band-structure calculation:

(a) The wave functions of the d-like electrons are slightly more diffuse in the metal than in the free atom. Confirmation of this comes from the experimental x-ray scattering form factors[12] which are found to be about 4% lower in the metal than calculated for the atom.

(b) The $4s$ wave functions are extremely diffuse.

(c) The electron configuration differs from that of the free atom, being closer to $3d^7 4s$ than to the atomic configuration $3d^6 4s^2$. Thus Callaway[7] and Stern[7] both found that the superposition of potentials derived from the atomic $3d^6 4s^2$ configuration produced $3d$ bands lying entirely below the $4s$ band, implying a configuration $3d^8$ in conflict with the starting configuration. Because of (a), the x-ray scattering form factor per electron is unknown, so it gives no direct confirmation of the number of electrons; however, the isomer shift has been interpreted in favor of the $3d^7 4s$ configuration (see Ingals[7]).

(d) Hybridization is important.

(e) The Slater exchange potential $\rho^{1/3}$ is unsatisfactory as a means of incorporating exchange. Arbitrary adjustments have to be made to it to fit the correct magnetic moment, which, for an understanding of magnetic properties, is an unsatisfactory procedure. There is an additional important consideration which necessitates avoiding it for this calculation. Consider the difference between the exchange potentials for the two spin states

$$\rho_\uparrow^{1/3} - \rho_\downarrow^{1/3}.$$

This always has the same sign as $\rho_\uparrow - \rho_\downarrow$, which is the spin density. In iron, the spin density is everywhere positive except in some regions in which the wave functions are small.[13] Hence, any expectation value

$$\langle \Psi | \rho_\uparrow^{1/3} - \rho_\downarrow^{1/3} | \Psi \rangle$$

is necessarily positive. By first-order perturbation theory this requires the minority-spin bands to be above the corresponding majority-spin bands

for all $\vec{k}$ values. However, several lines of experimental evidence[14-16] seem to indicate that the $4s$-like states are actually polarized negatively[17] with respect to the d states and therefore we must not inject into the calculation an unwarranted predisposition towards positive polarization.

In the band structure reported below, points (a), (b), and (d) are satisfied by choosing a variational method for finding wave functions and energies with a careful choice fo the trial wave function. The expression used was of the form

$$\Psi = \sum_{m=1}^{5} \lambda_m u_d^m(\vec{r}) + \sum_{i=1}^{19} \mu_i u_{\mathrm{OPW}}^i , \tag{1}$$

where λ_m and μ_i are the expansion coefficients and u_{OPW}^i are OPW wave functions; the 19 OPW's correspond to the 19 reciprocal lattice vectors out to the second nearest neighbors

$$\begin{aligned} u_d^m(\vec{r}) &= \textstyle\sum_n e^{i\vec{k}\cdot\vec{R}_n}\, \phi_d^m(\vec{r}-\vec{R}_n), \\ \phi_d^m(\vec{r}) &= [P_d(r)/r]\, C_2^m(\theta,\phi), \\ C_2^1 &= Y_2^0 , \\ C_2^2 &= (1/\sqrt{2})(Y_2^2 + Y_2^{-2}), \\ C_2^3 &= (-i/\sqrt{2})(Y_2^2 - Y_2^{-2}), \\ C_2^4 &= (i/\sqrt{2})(Y_2^1 + Y_2^{-1}), \\ C_2^5 &= (-1/\sqrt{2})(Y_2^1 - Y_2^{-1}), \\ Y_2^m &= \text{usual spherical harmonics.} \end{aligned} \tag{2}$$

The C_2^m are real functions which form bases for some representations of the cubic group. The choice of the function $P_d(r)$ is determined by point (c). Since the final configuration is expected to be near $3d^7 4s$, it seems that a certain amount of self-consistency is built in by choosing $P_d(r)$ to be the radial part of the d-wave function for the free-atom $3d^7 4s$ configuration. In making this choice, no restriction is implicit that the final wave functions have this particular radial behavior because the additional terms $u_{\mathrm{OPW}}(r)$ can easily alter the radial character, and in fact must do so in a spin-dependent fashion if the wave functions are to be spin dependent. By choosing the d function to be approximately correct, the demands placed on the OPW expansion are less acute.

The function $P_d(r)$ and the core functions ($1s$-$3p$) used in forming the OPW's were supplied for the configuration $3d^7 4s$ in an analytic form[18] by Gilbert.[19] The relevant parameters for $P_d(r)$ are given in Table I and for comparison the corresponding parameters for the atomic $3d^6 4s^2$ configuration are also listed. $P_d(r)$ for both cases are plotted in Fig. 1. It is seen that the $3d^7 4s$ function has a smaller amplitude than the $3d^6 4s^2$ function up to a radius of about 1.2 Bohr radii, and thereafter the $3d^7 4s$ function has the greater amplitude.

TABLE I. Parameters for the analytic expansion of the atomic $3d$ orbital. The wave function is $\psi_{3d}(\vec{r}) = \sum_{i=1}^{5} P_i r^2 e^{-\alpha_i r} [Y_2^m(\theta,\phi)]$, where $P_i = (6!)^{-1/2}(2\alpha_i)^{7/2} C_i$.

α	$C(3d^7\,4s)$	$C(3d^6\,4s^2)$
4.095 42	0.252 76	0.253 56
11.500 00	0.029 17	0.030 38
6.004 05	0.248 51	0.271 81
2.616 91	0.395 69	0.460 99
1.448 80	0.267 14	0.147 57

The presence of the OPW components in the trial wave function serves three purposes. In the first place, the wave functions of the s-like states, being fairly diffuse, are well approximated by OPW wave functions. Second, the OPW wave function can contain some d character and can contribute some components to the d-wave function, making their radial character fully state dependent. Third, hybridization of d- and s-like states is built into the wave function. If the λ_m are large and the μ_i small, we will have a purely d-like state. If μ_i are large and λ_m are small, wave functions of $4s$-$4p$-$\cdots$ character result. If both λ_m and μ_i are comparable, pure states no longer occur, and the wave function is a hybrid.

It should be noted that the basis functions in (1) are not orthogonal to one another. Thus, the secular equations to be solved for the energies E and wave functions are

$$|H - ES| = 0, \tag{3}$$

where S is a nondiagonal, but Hermitian, matrix of the unit operator. H is the Hamiltonian matrix.

Points (c) and (e) are incorporated into the band structure in the construction of H. Initially, assumptions were made about the distribution of population throughout the BZ to account for an approximate configuration $3d^7 4s$. However, the problem of greater magnitude was a realistic treatment of exchange. It was decided that here the general principle to be followed was to attempt to calculate the exchange matrix elements from the Hartree-Fock Hamiltonian as accurately as possible. In particular, approximations in terms of the substitution of some physical model, such as the local potential $\rho^{1/3}$, for the terms in question were avoided. Approximations of a mathematical nature, such as the truncation of a series expression, or limitation of multicenter integrals to two-center integrals, were made. One notable exception to this rule is the use of screened exchange for some s-state interactions, but this is dictated by the known difficulties with Hartree-Fock exchange for a system

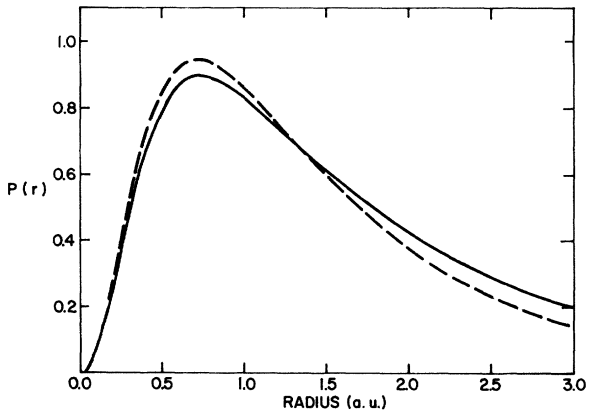

FIG. 1. Radial wave functions of d electrons in atomic iron. Curve I is for the $3d^7\ 4s$ configuration; curve II is for the $3d^6\ 4s^2$ configuration.

of free electrons.

Because exchange was treated without making localizing approximations, it is not possible to list a local potential which gives rise to the band structure. Rather, the matrix elements of H were calculated directly without the intermediary of a local potential.

Since energies at general points in the BZ were of interest to this problem as well as energies at symmetry points, no attempt was made to use group theory in the construction of the wave functions, it being more convenient to have just one set of computer programs that would handle all $\vec{k}$ points on an equal footing.

The lattice spacing assumed for this calculation was 2.86 Å.

III. BAND-STRUCTURE METHODOLOGY

In this section, the construction of the basic building blocks of the Hartree-Fock matrices is described. The assembling of these component parts into the final matrices is described in Sec. IV.

A. Exchange Matrix Elements

The general form of the exchange matrix elements is the negative of

$$\int \Psi_i^*(\vec{r}_1)\Psi_j(\vec{r}_1)(1/r_{12})\Psi_j^*(\vec{r}_2)\ \Psi_l(\vec{r}_2)\,d\tau_1\,d\tau_2/\int|\Psi_j|^2 d\tau\,, \tag{4}$$

where Ψ here has one of two forms, either a TB function

$$\Psi=(1/N^{1/2})\sum_n e^{i\vec{k}\cdot\vec{R}_n}u_{\vec{k}}(\vec{r}-\vec{R}_n) \tag{5}$$

or an OPW

$$\Psi=(1/V^{1/2})e^{i\vec{k}\cdot\vec{r}}-\sum_i b_{\vec{k}}^i\phi_c^i\,, \tag{6}$$

where ϕ_c^i is a TB core-state wave function and $b_{\vec{k}}^i$ is a constant chosen to make Ψ orthogonal to the core state.

It is clear that many types of integrals occur. To establish the terminology used here, we state that expression (4) is the exchange of the state l or i with the state j. Subsequently, a summation has to be made over the j states. The express forms of the integrals are given in Secs. III A 1–3.

1. *Exchange with d states*

Ψ_j has the form of Eq. (5). In all cases discussed below, spherical symmetry was explicitly invoked by assuming equal population of the states (2) for electron j.

a. Exchange of d states with d states. Here, both Ψ_i and Ψ_l have the form (2) and $\vec{k}_i=\vec{k}_l$. Using standard manipulations, the integrals may be expressed as a sum of one- to four-center integrals. The approximation is made that integrals involving three or more centers are negligible on the grounds that two-center integrals are sufficiently small. Typical values for the overlap integrals for first- to fourth-nearest-neighbor overlaps are 0.02, 0.015, 0.001, and 0.0001.

In addition, certain two-center integrals were neglected due to reasons described below. The remaining terms were

$$\frac{1}{N}\int u^{m_i*}(\vec{r}_1)u^{m_j}(\vec{r}_1)\,\frac{1}{r_{12}}$$
$$\times u^{m_j*}(\vec{r}_2)u^{m_l}(\vec{r}_2)\,d\tau_1\,d\tau_2\ \text{(one center)}, \tag{7}$$

$$\frac{1}{N}\sum_n e^{-i\vec{k}_i\cdot\vec{R}_n}\int u^{m_i*}(\vec{r}_1-\vec{R}_n)u^{m_j}(\vec{r}_1)\,\frac{1}{r_{12}}$$
$$\times u^{m_j*}(\vec{r}_2)u^{m_l}(\vec{r}_1)\,d\tau_1\,d\tau_2\ \text{(two center)}. \tag{8}$$

Terms rejected were of the form

$$\frac{1}{N}\sum_n e^{-i\vec{k}_j\cdot\vec{R}_n}\int u^{m_i*}(\vec{r}_1)u^{m_j}(\vec{r}_1)\frac{1}{r_{12}}$$
$$\times u^{m_j*}(\vec{r}_2-\vec{R}_n)u^{m_l}(\vec{r}_2)\,d\tau_1\,d\tau_2\,, \tag{9}$$

$$\frac{1}{N}\sum_{n,p} e^{-i\vec{k}_i\cdot\vec{R}_n}e^{-i\vec{k}_j\cdot\vec{R}_p}\int u^{m_i*}(\vec{r}_1)u^{m_j}(\vec{r}_1)\,\frac{1}{r_{12}}$$
$$\times u^{m_j*}(\vec{r}_2-\vec{R}_p)u^{m_l}(\vec{r}_2-\vec{R}_n)\,d\tau_1\,d\tau_2\,, \tag{10}$$

$$\frac{1}{N}\sum_{n,p} e^{-i\vec{k}_i\cdot\vec{R}_n}e^{-i\vec{k}_j\cdot\vec{R}_p}\int u^{m_i*}(\vec{r}_1-\vec{R}_n)u^{m_j}(\vec{r}_1)\,\frac{1}{r_{12}}$$
$$\times u^{m_j*}(\vec{r}_2-\vec{R}_p)u^{m_l}(\vec{r}_2)\,d\tau_1\,d\tau_2\,, \tag{11}$$

$$\frac{1}{N}\sum_n\int u^{m_i*}(\vec{r}_1-\vec{R}_n)u^{m_j}(\vec{r}_1)\frac{1}{r_{12}}$$
$$\times u^{m_j*}(\vec{r}_2)u^{m_l}(\vec{r}_2-\vec{R}_n)\,d\tau_1\,d\tau_2\,. \tag{12}$$

It is seem that (8) and (9) are similar; the reason one is retained and the other is not lies in the significance of the subscripts i and j. The reason for neglecting (9) is that to some extent it is canceled

by the terms arising from the binomial expansion of the denominator term in (4). In addition, we recall that a sum over j has to be performed, and for small terms such as these, it should be reasonable to take the full BZ result and scale it according to the population. However, because the integrals are $\vec{k}$ independent, the summation is proportional to $\sum e^{i\vec{k}_j \vec{R}_n} \equiv 0$. The summation argument also applies to (10) and (11), and in any case these terms along with (12) are probably smaller by the order of an overlap integral than the ones retained. In addition, (9)–(12) can be interpreted in terms of the exchange interaction causing a double electron excitation from one atomic site to another, an effect which should be minimized by exchange screening.[20]

The two-center integrals were reduced to one-center form by expanding the wave function of the electron on the second site (site B) in a series of functions centered on the first site (site A), using a method based on an analytic expansion[21] of Löwdin's "α function"[22] and standard forms of the rotation matrices[23] for spherical harmonics. Two-center integrals out to fourth nearest neighbors were included, although the contributions from third and fourth neighbors were negligible.

b. Exchange of OPW *states with d states.* For the parts of the exchange involving two plane waves, one each from Ψ_i and Ψ_l, the potential e^2/r_{12} was Fourier analyzed and lattice summations and angular integrals performed analytically, the final expression being

$$\sum_{\vec{K}} \left(\frac{4\pi}{\Omega}\right)^2 \frac{5}{N} S \int r P_d(r) j_2(|\vec{k}_i - \vec{k}_l + \vec{k}_j + \vec{K}|\, r) dr \times \int r P_d(r) j_2(|\vec{k}_j + \vec{K}|\, r)\, dr \frac{1}{|\vec{k}_j - \vec{k}_l + \vec{K}|^2 + \alpha^2}, \tag{13}$$

where

$$S = \frac{4\pi}{5} \sum_m \frac{1}{N_m} C_2^m(\theta_{k_i}, \phi_{k_i}) C_2^m(\theta_{k_l}, \phi_{k_l}),$$

N_m is the normalization integral for the state of angular symmetry C_2^m, $\vec{K}$ is the reciprocal lattice vector, and j_2 is the spherical Bessel function of order 2.

A convergence test was performed and it was found that the series (13) was well converged when summed over 141 shortest $\vec{K}$ vectors. This set of vectors was then used for the computation of the required matrix elements.

Expression (13) gives the matrix elements for exchange with d state Ψ_j. A practical scheme for summing over the Avagadro's number of states Ψ_j has to be found. In this case, the method employed was to choose a set of 97 $\vec{k}$ vectors throughout the BZ, as uniformly spaced as was conveniently possible, to be representative of all states. These will be referred to as sample states. The matrix elements (13) were calculated for each of the $\vec{k}$ vectors, and each multiplied by a weighting factor assigned to the $\vec{k}$ vector. The weighting factors were assigned on the basis of the volume of an element of the BZ allocated to and containing the $\vec{k}$ point in question. Further population factors were assigned to each $\vec{k}$ point as discussed in Sec. VI, and the final matrix elements found by adding the contributions from each sample state. This method has been used before by Phillips and Kleinman.[24]

The constant α^2 in the denominator of (13) has the mathematically important role of eliminating a divergence which would otherwise occur in the neighborhood of $\vec{k}_l = \vec{k}_j + \vec{K}$. Physically it corresponds to a static wave-number–independent screening factor. That is, the Coulomb potential $1/r_{12}$ is replaced with the screened potential $e^{-\alpha r}/r_{12}$. While a dielectric treatment can be adequate for fairly free electrons,[20,25] such as the conduction electrons in a metal, it is not an adequate process for d-like states.[4] Unfortunately, no treatment of the correlation of the d states with the $4s$ states has been given, but it seems that the screened Coulomb potential would have limited applicability. Accordingly, it was determined that α should be a small quantity chosen only to avoid the divergence. A sphere of volume equal to a typical elemental volume associated with a sample $\vec{k}$ vector was considered. Suppose its radius is q_0. Then α is chosen so that

$$\int \frac{d\vec{q}}{q^2} = 4\pi q_0 = \frac{\frac{1}{3}\pi q_0^3}{\alpha^2} \quad . \tag{14}$$

That is, at a potential divergence, the same result is obtained for the Fourier inversion integral over the sphere by (i) moving the origin to the center of the sphere and using the unscreened Coulomb potential and (ii) selecting the center of the sphere to be representative of all points in the sphere using the screened potential. On this basis $\alpha = 0.1$. Since it is a small quantity, it was assumed that no violence is done by including it in expression (13) even away from points of near divergence.

For the terms in which Ψ_i contributes a plane wave and Ψ_l contributes a core wave function $u_c(\vec{r}_2)$, the small overlap of core functions on one site with d functions on another site was invoked to restrict the integral to the Fourier transform of a one-center integral

$$u_j(\vec{r}_1) \int u_j^*(\vec{r}_2)[u_c(\vec{r}_2)/r_{12}]\, d\tau_2 .$$

Standard techniques are available for this type of integral and for the type of integral which occurs when both OPW states contribute core terms. In the latter case a simple atomlike one-center integral results.

c. Hybrid matrix elements of exchange with d states. The generic form is (4) with Ψ_i = OPW and

Ψ_i = TB function. As in Sec. III A 1 a, any two centeredness of Ψ_j is rejected. The one-center contribution involving a plane wave was handled in the same way as terms involving a single core and single plane wave were treated in Sec. III A 1 b.

The two-center part was again reduced to a form similar to a one-center integral by expanding the d function from Ψ_i on site B about the site A using the α-function technique. The plane wave was expanded in terms of spherical Bessel functions and spherical harmonics. Both expansions are, in principle, infinite; but for computational purposes, only components up to an angular momentum of 2 were taken. The reason for expecting this to be adequate lies in the behavior of the α-function expansion, particularly in the region where the d functions overlap. For increasingly higher angular-momentum components, the amplitude of the α functions decreases for radius values other than those near the interatomic distance.

The same α-function expansion was used to calculate terms such as

$$\int u_i^{c*}(\vec{r}_1) u_j^d(\vec{r}_1)(1/r_{12}) u_j^d(\vec{r}_2) u_l^d(\vec{r}_2 - \vec{R}_n)\, d\tau_1\, d\tau_2 ,$$

where u_i^c is a core-function component of Ψ_i. Two-center contributions were taken only as far as second nearest neighbors.

2. *Exchange with* OPW *states*

Here Ψ_j has the form of (6).

a. Exchange of d states with OPW *states.* Both Ψ_i and Ψ_l have the form of (5). For those terms in which Ψ_j contributes one or two core terms, techniques discussed in Sec. III A 1 c were applied. For the case in which Ψ_j contributes two plane waves, the Coulomb potential e^2/r_{12} was Fourier analyzed, and, as before, lattice summations and angular integrals were performed analytically. The resulting expression is

$$\sum_K \left(\frac{4\pi}{\Omega}\right)^2 \frac{4\pi}{N} C_2^{mi}(\theta_{\vec{k}_i}, \phi_{\vec{k}_i}) C_2^{ml}(\theta_{\vec{k}_l}, \phi_{\vec{k}_l}) \times \left| \int r P_d(r) j_2(|\vec{k}_j + \vec{K}|\, r)\, dr \right|^2 \times \frac{1}{|\vec{k}_j - \vec{k}_l + \vec{K}|^2 + \alpha^2} \quad . \tag{15}$$

Again, the summation over reciprocal lattice vectors was carried out over 141 reciprocal lattice vectors. The set of sample states and weighting factors, and the same value of α, were employed as in Sec. III A 1 b.

b. Exchange of OPW *states with* OPW *states.* Here Ψ_i and Ψ_l have the form (6).

Again, a screened Coulomb potential is used, but in this case with some more justification[20,25] than for the cases previously discussed. It is recognized that using a static wave-number–independent screening constant is an oversimplification. However, because of the exploratory nature of this problem, it was decided to avoid excessive complication which would be necessary to incorporate a more realistic dielectric function. The value chosen for α was that given by the Thomas-Fermi model, in this case determined by a conduction ($4s$) electron density of one electron per atom in accordance with a configuration of $3d^7 4s$. The value taken for α was 1.0.

There are many types of terms. With no core terms present the contribution is

$$\frac{4\pi}{V} \frac{S_j^{-1}\, \delta_{il}}{(\vec{k}_l - \vec{k}_j)^2 + \alpha^2} \quad . \tag{16}$$

Contributions from terms containing one core reduce to the form

$$-\frac{4\pi}{V} \frac{b_{\vec{k}_i}^c}{\Omega^{1/2}} \frac{S_j^{-1}}{(\vec{k}_l - \vec{k}_j)^2 + \alpha^2} \int e^{i\vec{k}_l \cdot \vec{r}}\, u_i^{c*}(\vec{r})\, d\vec{r} \tag{17}$$

and

$$-\frac{4\pi}{V} \frac{b_{\vec{k}_j}^c}{\Omega^{1/2}} \frac{S_j^{-1}}{(\vec{k}_l - \vec{k}_j)^2 + \alpha^2} \int e^{i(\vec{k}_j + \vec{k}_l - \vec{k}_i)\cdot \vec{r}}\, u_j^{c*}(\vec{r})\, d\vec{r} \quad . \tag{18}$$

In these terms S_p is a normalization integral $S_p = 1 - \sum_c |b_{\vec{k}p}^c|^2$.

For the terms involving two core terms, the contributions were approximated by the $\vec{k}_j = 0$ values. Terms so approximated had the following forms:

$$b_{\vec{k}_j}^{c'*} b_{\vec{k}_i}^{c*} \frac{4\pi}{V} S_j^{-1} \sum_{\vec{K}} \frac{1/\Omega}{(\vec{k}_l - \vec{k}_j + \vec{K})^2 + \alpha^2} \times \int d\vec{r}_1\, e^{i(\vec{k}_l + \vec{K})\cdot \vec{r}_1} u_i^{c*}(\vec{r}_1) \int d\vec{r}_2\, e^{i(\vec{k}_j - \vec{K})\cdot \vec{r}_2} u_j^{c'*}(\vec{r}_2), \tag{19}$$

$$b_{\vec{k}_l}^{c'} b_{\vec{k}_i}^{c*} \frac{4\pi}{V} S_j^{-1} \sum_{\vec{K}} \frac{1/\Omega}{(\vec{k}_l - \vec{k}_j + \vec{K})^2 + \alpha^2} \times \int d\vec{r}_1\, e^{i(\vec{k}_l + \vec{K})\cdot \vec{r}_1} u_i^{c*}(\vec{r}_1) \int d\vec{r}_2\, e^{-i(\vec{k}_l + \vec{K})\cdot \vec{r}_2} u_l^{c'}(\vec{r}_2), \tag{20}$$

$$b_{\vec{k}_j}^{c} b_{\vec{k}_j}^{c'*} \frac{4\pi}{V} S_j^{-1} \sum_{\vec{K}} \frac{1/\Omega}{(\vec{k}_l - \vec{k}_j + \vec{K})^2 + \alpha^2} \times \int d\vec{r}_1\, e^{i(\vec{k}_l - \vec{k}_i - \vec{k}_j + \vec{K})\cdot \vec{r}_1} u_l^{c}(\vec{r}_1) \int d\vec{r}_2\, e^{i(\vec{k}_j - \vec{K})\cdot \vec{r}_2} u_j^{c'*}(\vec{r}_2), \tag{21}$$

$$b_{\vec{k}_i}^{c} b_{\vec{k}}^{c'} \frac{4\pi}{V} S_j^{-1} \frac{1/\Omega}{(\vec{k}_l - \vec{k}_j)^2 + \alpha^2} \times \int d\vec{r}\, e^{i(\vec{k}_l - \vec{k}_j)\cdot \vec{r}}\, u_i^{c}(\vec{r})\, u_j^{c'}(\vec{r}). \tag{22}$$

Again summations over reciprocal lattice vectors were taken to 141 terms. Terms involving three or four core terms were ignored.

c. Hybrid matrix elements of exchange with OPW *states.* Here we take Ψ_i = TB function, Ψ_l = OPW.

In the manner similar to that above, the relevant forms are

$$\frac{4\pi}{V}\frac{1}{(\vec{k}_l-\vec{k}_j)^2+\alpha^2}\,S_j^{-1}\left[\frac{1}{\Omega^{1/2}}\int e^{i\vec{k}_l\cdot\vec{r}}\,u_d^*(\vec{r})\,d\vec{r}\right],$$

$$-\frac{4\pi}{V}\,b^c_{\vec{k}_l}\,S_j^{-1}\sum_{\vec{K}}\frac{1}{(\vec{k}_i-\vec{k}_j+\vec{K})^2+\alpha^2} \tag{23}$$

$$\times\left[\frac{1}{\Omega^{1/2}}\int e^{i(\vec{k}_l+\vec{K})\cdot\vec{r}_1}\,u_d^*(\vec{r}_1)\,d\vec{r}_1\right]$$

$$\times\left[\frac{1}{\Omega^{1/2}}\int e^{-i(\vec{k}_l+\vec{K})\cdot\vec{r}_2}\,u_l^c(\vec{r}_2)\,d\vec{r}_2\right], \tag{24}$$

$$-\frac{4\pi}{V}\,b^c_{\vec{k}_j}\,S_j^{-1}\sum_{\vec{K}}\frac{1/\Omega}{(\vec{k}_l-\vec{k}_j+\vec{K})^2+\alpha^2}$$

$$\times\int d\vec{r}_1\,e^{i(\vec{k}_l+\vec{K})\cdot\vec{r}_1}\,u_d(\vec{r}_1)$$

$$\times\int d\vec{r}_2\,e^{i(\vec{k}_j-\vec{K})\cdot\vec{r}_2}\,u_j^c(\vec{r}_2). \tag{25}$$

For these terms α was taken as 0.5, i.e., about midway between 1.0 and 0.1.

3. *Exchange with Core States*

Here Ψ_j is a TB function formed out of atomic core states. It is always assumed that core states on different atomic sites do not overlap.

a. Exchange of d states with core states. The formulas here are the same as expressions (7) and (8) with $u^m{}_j$ being replaced by the appropriate core functions.

b. Exchange of OPW *states with core states.* Since core states were provided in a suitable analytic form, a method due to Brinkman and Goodman[26] could be used for the parts involving two plane waves. The characteristic features of this method are the Fourier analysis of the Coulomb potential $1/r_{12}$ coupled with an explicit analytic summation over the full BZ for the state Ψ_j. That is, the fact that core states are fully occupied could be exploited so that no sampling procedure had to be assumed, and no screening constant need be inserted. Brinkman and Goodman develop an analytic expression for the exchange integral involving an expansion in Legendre polynomials $P_l(\cos\theta)$, where θ is the angle between the wave vectors of the two plane-wave states. A convergence test showed that only $l=0$ and $l=1$ need be considered in the present problem. Computationally, the procedure was found to be time consuming, so that it is not unattractive to use a direct approach in which the plane waves are expanded in terms of spherical harmonics and spherical Bessel functions and the radial integrals performed numerically in the usual way.

Terms in which the OPW states contribute one or two core states were treated as in Sec. III A 1 b with the appropriate change of *d* states to core states.

c. Hybrid matrix elements of exchange with core states. Techniques discussed in Secs. III A 1 a (for no plane waves) and III A 1 b (one plane wave) were readily adapted to the evaluation of these terms.

B. Matrix Elements of Coulomb Interaction

Since, in the Hartree-Fock approximation, the Coulomb terms are derived from a local potential, the matrix elements are simpler to evaluate than the exchange matrix elements. However, the basic usefulness of the techniques of α-function expansions for the *d* states and Fourier transformation for the plane-wave states remains.

The basic expression is

$$\int\Psi_i^*(\vec{r}_1)\;\Psi_i(\vec{r}_1)(1/r_{12})\,|\Psi_j(\vec{r}_2)|^2\,d\tau_1\,d\tau_2/\int|\Psi_j(\vec{r})|^2\,d\tau. \tag{26}$$

The charge densities $|\Psi_j|^2$ are easily constructed for the core states, and consist of a spherically symmetric distribution centered on the lattice sites. The *d*-state charge density is also taken to be spherically symmetric, but in this case the charge distributions on each site can overlap slightly. For reasons similar to those in Sec. III A 1 a, the interference terms $u_d^j(\vec{r})\;u_d^j(\vec{r}-\vec{R}_n)$ are ignored.

The charge density of the 4*s*-like states was obtained by assuming that it can be approximated by the integrated charge density of single OPW states occupying the interiors of two spherical Fermi surfaces – one for each spin. The radii of the spheres were chosen to match an assumed population as discussed in Sec. IV. Initially the charge density was calculated throughout a sphere equal in volume to the unit cell and centered on the lattice sites. Such spheres necessarily overlap, and in the region of overlap the charge density is overemphasized. Conversely, there are some interstitial regions to which no charge has been allocated. To correct for this deficiency a correction potential ϕ was calculated,

$$\phi=a(\phi_1-\phi_2), \tag{27}$$

where ϕ_1 is the potential due to one proton at each lattice site and a uniform distribution of electrons corresponding to one electron per proton, ϕ_2 is a potential due to one proton at each lattice site surrounded by a charge of one electron uniformly distributed throughout a sphere equal in volume to the unit cell, and a represents a scaling factor to account for the actual population. The formulas are taken from Gaspari[27]:

$$\phi_1=\phi_1'+\phi_1'',$$

$$\phi_1'=\frac{3}{4\eta r_s^3}-\frac{3}{10r_s}-\sum_n\frac{\operatorname{erfc}(|\vec{r}-\vec{R}_n|/\sqrt{\eta})}{|\vec{r}-\vec{R}_n|},$$

$$\phi_1''=-\frac{3}{r_s^3}\sum_{K\neq0}K^{-2}\,e^{i\vec{K}\cdot\vec{r}-\vec{K}^2/4\eta},$$

$$\phi_2=\textstyle\sum_n\;(\vec{r}-\vec{R}_n),$$

$$V(\mathrm{r}) = \left[-\frac{1}{r} + \frac{1}{2r_s^3}(3r_s^2 - r^2)\right], \quad r \leq r_s$$
$$= 0, \quad r > r_s$$

where r_s is the radius of the Wigner-Seitz sphere. The potentials ϕ_1 and ϕ_2 are independent of the choice of the parameter η. It is chosen on the basis of giving rapid convergence. This potential ϕ turned out to be very small compared to the spherically symmetrical potential.

The matrix elements of the potentials due to the core- and d-state charge distributions are calculated in a straightforward manner. For the matrix elements of the s-state charge density some simple special modifications were made to the standard procedures. Consider contributions such as

$$\int u_d^*(\vec{r}_1) u_d(\vec{r}_1 - \vec{R}_n) \left| \Psi_{\mathrm{OPW}}(\vec{r}_2) \right|^2 / r_{12} \, d\tau_1 \, d\tau_2 \, . \qquad (28)$$

For $\vec{R}_n$ equal to a nearest-neighbor displacement, the correction potential as calculated along a (1, 1, 1) line was added to the spherically symmetric part of the potential, since only the potential in the overlap region, in this case the region around the (1, 1, 1) line, should be important. Similarly, for $\vec{R}_n$ equal to a second-nearest-neighbor displacement, the correction potential along the (1, 0, 0) direction was used. For matrix elements between plane waves, the Fourier transform of ϕ'' is calculated analytically, and both ϕ_1' and ϕ_2 are easily expressed as superpositions of spherically symmetrical potentials, which are then easily Fourier transformed.

The potential due to the nuclear charges was added to the spherically symmetrical components due to the electrons prior to the evaluation of the matrix elements. In this way we sum over neutral units and so a rapidly convergent expansion on terms of multicenter integrals could be obtained when Ψ_i or Ψ_t were d states. In particular, contributions from third and fourth nearest neighbors were negligibly small. If the Coulomb potential is represented as $V(r)$, two types of two-center terms occur and both were included:

$$\int u_i^{d*}(\vec{r}) V(r) u_i^d(\vec{r} - \vec{R}_n) \, d\tau \, ,$$
$$\int u_i^{d*}(\vec{r} - \vec{R}_n) V(r) u_i^d(\vec{r} - \vec{R}_n) \, d\tau \, .$$

The second of these represents the electrostatic field in the neighborhood of one site due to all the charges on other sites; that is, it is the "crystal-field" term.

Because the Coulomb potential has been reduced to a combination of local spherically symmetric potentials, the calculation of hybrid matrix elements presented no particular difficulty, being simple adaptations of the techniques already discussed.

IV. ASSEMBLING HARTREE-FOCK HAMILTONIAN MATRIX

Ideally, for Coulomb and exchange contributions to the Hartree-Fock Hamiltonian for a given state, the wave functions of every (Avogadro's number) occupied state should be known and the individual contributions due to them totaled. Of course, this is impractical, so a sampling technique has been used. However, even though this method reduces the number of individual calculations to something tractable, prior to the actual band calculation the wave functions are unknown, so assumptions about them have to be made also.

From the outset, it has been recognized that conduction-electron wave functions are mixtures of both s and d character, the particular admixtures having to be found from the calculation. Unfortunately, this is still too complex a description to incorporate into the calculation, so further simplification is necessary. For the purposes of this calculation the idea of hybridization is incorporated in the following approximate fashion. Each electron state at each sample $\vec{k}$ point was subjectively estimated to characterize, say, m d states and n $4s$ states, where $m + n = 1$. Thus, the Coulomb and exchange matrix elements due to these states are calculated on the basis of pure d states or pure single OPW states and these multiplied by the subjectively obtained population factors m and n. Of course, the over-all weighting factors representing the size of the volume element of the BZ associated with the sample $\vec{k}$ point were also used.

The Appendix shows how the sample points were chosen. The basis of the subjective estimates was the band calculation of Wakoh and Yamashita.[8] The allocation for majority-spin d states was particularly simple. There is one vacant state between H and N and all other d states are present nearly everywhere else on this line. Thus, the weighting factor for point 5 (see the Appendix) is taken as 0.8. All five d states are occupied at Γ, so a weighting factor of 1.0 is allocated to point 1 and similarly to points 2–4. The population for point 6 was chosen to bring the total number of majority-spin d states to 4.7, and reflects a small depopulation between N and P.

The allocations for the minority-spin d states were more difficult. For example, in deciding the weighting factors for the 3 points, we assume that they represent the points between 0.4 and 0.6 of the distance from Γ to the BZ surface. In going from Γ to N, two of the states which are triply degenerate at Γ are present between 40 and 60% of the ΓN line, and the third is not. Neither of the doubly degenerate states at Γ is present. In going from Γ to P, two of the triply degenerate states at Γ are occupied. The other leaves the Fermi surface, but by virtue of hybridization with the OPW states, the d character reappears below the Fermi surface about 50% of the distance from Γ to P. Thus, this state is considered to be half present

in the region from 40 to 60%. In going from Γ to H, two of the three triply degenerate and one of the doubly degenerate states at Γ are taken as present in the interval. The average number of states present is $\frac{1}{3}(2+2.5+3)=2.5$ for a weighting factor of 0.5. Of course, this approach is quite approximate, so minor adjustments are made to the weighting factors to produce the total population given by Wakoh and Yamashita.

For the s-state populations, spherical Fermi surfaces were assumed. Starting from Γ, states were filled with a weighting factor of 1 until the point was reached where a smaller weighting factor had to be assigned to keep the total from exceeding the predetermined population.

The weighting factors as determined by the above method are listed in Table II. As discussed in Sec. VI, the band shapes that result from the present calculation differ from those of Wakoh and Yamashita, but the weighting factors as determined by the above method would not change very significantly. Hence, this calculation is essentially self-consistent, with one minor exception. Since earlier work indicated that there is the possibility of a negative $4s$ polarization, the $4s$ population was taken as 0.4 majority spins and 0.5 minority spins. No evidence was found here for a negative spin polarization, but this discrepancy should not be serious.

There are some parts of the Hamiltonian which do not require the use of the sample states but which require instead the total populations to be inserted. Examples of this are the Coulomb potentials due to both s and d states, and the exchange matrix elements of d states with d states. The total populations are as indicated in Table II.

TABLE II. Population weighting factors assigned to the points listed in the Appendix.

Point	Majority d	Minority d	Majority s	Minority s
1	1	0.6	1.0	1.0
2	1	0.57	1.0	1.0
3	1	0.53	1.0	1.0
4	1	0.5	0.621 620 3	0.959 457 8
5	0.8	0.38	0	0
6	0.954 094 6	0.5	0	0
Total No. of states	4.7	2.4	0.4	0.5

V. CORRELATION CORRECTIONS

As is well known, the Hartree-Fock approximation replaces the (dynamic) Coulomb interaction between electrons with the Coulomb potential of a static averaged charge cloud. Any departures from this picture that occur in reality are called correlation effects. Several formal treatments of the many-body problem have been given, and several of the relevant papers are reproduced in the book by Pines.[20] A necessary distinction has to be made between the treatment required for diffuse electrons such as the $4s$ states and that required for highly localized states such as the $3d$ electrons. For the former, the method of Hedin[3] is used, and for the latter a treatment by Hubbard[4] is relevant.

The role of correlation for the quasifree $4s$ electrons is to screen the exchange[20,25]; this was incorporated into the calculations via a static wave-number–independent dielectric function. Hedin showed that if a static approximation to the dielectric function is made, then the screened exchange must be augmented with a "Coulomb hole." For an electron gas of uniform density the Coulomb-hole potential is a constant:

$$V_{\mathrm{CH}}(\vec{r})=\frac{1}{2}\int\frac{d^3q}{(2\pi)^3}\,v(\vec{q})\left[\frac{1}{\epsilon(\vec{q},0)}-1\right], \tag{29}$$

where $v(\vec{q})$ is the Fourier component of the Coulomb potential e^2/r_{12}. For OPW wave functions, some $\vec{k}$ dependence is introduced and the approximate expression is

$$\begin{aligned}&V_{\mathrm{CH}}(\vec{r})\,\psi_{\vec{k}}(\vec{r})\\&=\frac{1}{2}\int\frac{d^3q}{(2\pi)^3}\,d^3\vec{r}\,'v(\vec{q})\left[\frac{1}{\epsilon(\vec{q},0)}-1\right]\\&\times e^{i\vec{q}\cdot(\vec{r}-\vec{r}\,')}\left[\delta(\vec{r}-\vec{r}\,')-\sum_c\Psi_c^*(\vec{r}\,')\,\Psi_c(\vec{r})\right]\psi_k(\vec{r}\,'),\end{aligned} \tag{30}$$

where Ψ_c is a TB core function.

Mahanti[28] has explored this approximation for cesium metal and finds the $\vec{k}$ dependence of (30) very feeble. Accordingly, (29) was used instead of (30). The matrix elements of V_{CH} were added to the Hartree-Fock Hamiltonian wherever the screened exchange was used, with the appropriate values of the screening constant in each case.

The correlation correction for d states is based on the conception that the dominant influence of correlation is to introduce localization properties into an otherwise itinerant picture, as discussed theoretically by Hubbard,[4] Kanamori,[29] and Gutzwiller.[30] Consider the one-center term in the expression for the exchange of a d electron with other d electrons in an itinerant picture:

$$\sum_{j\neq i}\frac{1}{N}\int u_i^*(1)\,u_j(1)\,\frac{1}{r_{12}}\,u_j^*(2)\,u_i(1)\,d\tau_1\,d\tau_2. \tag{31}$$

The summation over j goes over all electrons other than the state of interest, i.e., over $N'-1$ electrons, where N' is of the order of Avagadro's number. If the state is localized, the summation goes over only the other electrons on the given site and there is no factor $1/N$ multiplying the expression; i.e., the summation is over $N''-1$ states, where N'' is of the order of the number of electrons per atom, ≈ 5 for majority spin, ≈ 3 for minority

spin. Neglecting the difference between $N'-1$ and N', we see that the itinerant model differs from the local model by the inclusion of a self-exchange.

To illustrate the impact of this, consider the approximation used to create spherical symmetry for the one-center exchange terms; the expression for a half-filled atomic shell is used and scaled according to the population. The expression for a filled half-shell consists of two parts, a term identical in magnitude to the self-Coulomb term, V_c, and an expression identified as the exchange due to the other states, V_0. On the itinerant model, the exchange terms are then

$$-\tfrac{1}{5}n_\uparrow(V_c+V_0), \tag{32}$$

where $n_\uparrow$ is the band population of states with a given spin; $n_\downarrow$ is defined similarly for states with the opposite spin. The total Coulomb and exchange terms are

$$(n_\uparrow+n_\downarrow)V_c-\tfrac{1}{5}n_\uparrow(V_c+V_0). \tag{33}$$

For the fully localized model, the self-Coulomb and self-exchange terms are first canceled and then the exchange proportioned according to population

$$[(n_\uparrow-1)+n_\downarrow]V_c-\tfrac{1}{4}(n_\uparrow-1)V_0\,. \tag{34}$$

The difference between (33) and (34) is

$$(n_\uparrow-5)(\tfrac{1}{5}V_c-\tfrac{1}{20}V_0) \tag{35}$$

and is zero for a filled half-shell $n=5$. The energy (35) would represent the correlation energy if correlation effects were so strong that complete localization occurs. The integral V_0 is much smaller than the integral V_c, so in the following V_0 will be disregarded.

The correct picture[31] is intermediate between the extremes of full localization (zero bandwidth) and full itinerancy (finite bandwidth). Hubbard examined correlation effects in narrow s bands and has given the following expression for the effective exchange integral:

$$-V_{eff}=-V_c\frac{\frac{1}{4}\Delta}{[(\frac{1}{2}V_c+\frac{1}{4}\Delta)^2-\frac{1}{4}n\Delta V_c]^{1/2}}\,, \tag{36}$$

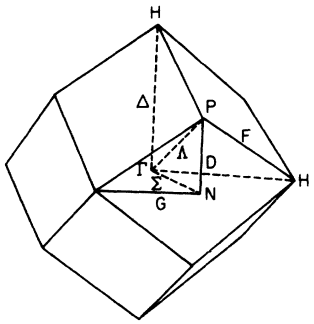

FIG. 2. Brillouin zone for the bcc lattice.

where Δ is the bandwidth and $n=\frac{1}{2}(n_\uparrow+n_\downarrow)$. Although lacking in rigorous justification, it seems reasonable that the generalization to d bands of (36) given by putting $n=\frac{1}{10}(n_\uparrow+n_\downarrow)$ should at least gauge the correlation energy contribution, so this approach is used here. Note that in the limit of zero bandwidth, (36) reduces the effective self-exchange integral to zero in accordance with the localized picture discussed above, and in the limit of very large Δ we recover an effective exchange energy equal to the self-exchange integral V_c.

Starting from the fully localized picture of zero self-exchange, the exchange interaction used here was found by adding $-\frac{1}{5}n_\uparrow V_{eff}$ to (33). It is recognized that the disappearance of the self-exchange interaction in going from itinerancy to locality is accomplished at the expense of the Coulomb interaction, so that, in replacing part of the self-exchange, to be consistent, the corresponding part of the Coulomb energy must be replaced, so a further V_{eff} is added to the total energy. The net form of the one-center interaction is, therefore,

$$[(n_\uparrow-1)+n_\downarrow]V_c-\tfrac{1}{4}(n_\uparrow-1)V_0+(1-\tfrac{1}{5}n_\uparrow)V_{eff}\,. \tag{37}$$

The contributions from multicenter integrals are regarded as being intrinsically real manifestations of itinerancy; that is, they represent genuine band effects which remain as a residue of itinerancy after the localization of correlation has been im-

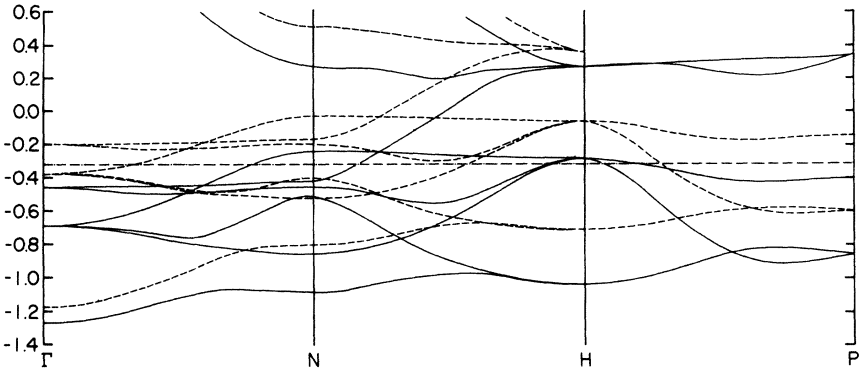

FIG. 3. Band structure for ferromagnetic iron in the ΓN, NH, and HP directions. The solid curves are for majority spin and the dotted curves are for minority spin. The energies are given in Ry. The Fermi level is the horizontal line at -0.314 Ry.

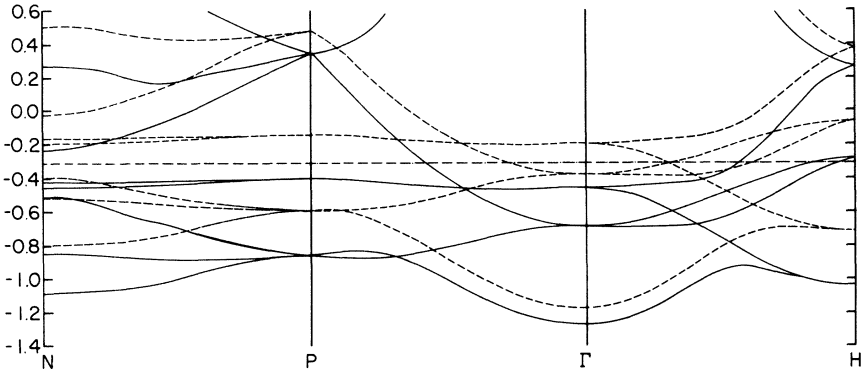

FIG. 4. Band structure for ferromagnetic iron in the NP, $P\Gamma$, and ΓH directions. The solid curves are for majority spin and the dotted curves are for minority spin. The energies are given in Ry. The Fermi level is the horizontal line at -0.314 Ry.

posed. Accordingly, they are scaled with respect to population in an analogous manner to Eq. (33).

For computational purposes, it is necessary to assume a value of Δ to insert in Eq. (36). This was initially taken by inspection of Wakoh and Yamashita's bands[8] to be 0.4 Ry. Subsequent to a first-band calculation, it was found that the present calculation produced wider bands than Wakoh and Yamashita, so the calculation was reiterated with $\Delta = 0.55$ Ry.

VI. SHAPES OF BANDS

The method described in the previous sections was used to calculate energies and wave functions at 110 inequivalent points in $\frac{1}{48}$ of the BZ, including 46 points along the symmetry lines joining the points Γ, N, H, and P (see Fig. 2). Two complete band structures were calculated corresponding to $\Delta = 0.4$ and $\Delta = 0.55$ Ry. The energy bands for the case $\Delta = 0.55$ Ry are depicted in Figs. 3 and 4. A convergence test was carried out at each point by including in the wave function five d states and one, thirteen, and nineteen OPW states successively. Table III lists the results at some symmetry points. It is seen that the convergence is generally excellent, but at the points P and H, states which should be degenerate may differ in energy by up to 0.01 Ry. The reason for this is that the same set of 19 reciprocal lattice vectors was used at all $\vec{k}$ points. While the set may give the correct angular character at Γ, at other points the set lacks some vectors necessary to meet the proper symmetry conditions. Fortunately, the deviation is small.

TABLE III. Results of a convergence test. Energies were calculated using five d states and one OPW, five d states and 13 OPW's, and five d states and 19 OPW's. The six lowest energies (in Ry) are listed for each case. Only the results for majority spin are listed.

	$5d+1$ OPW	$5d+13$ OPW	$5d+19$ OPW
Γ	−0.397	−0.432	−0.457
	−0.398	−0.432	−0.457
	−0.630	−0.690	−0.690
	−0.630	−0.690	−0.690
	−0.630	−0.690	−0.690
	−1.272	−1.272	−1.272
N	−0.178	−0.234	−0.239
	−0.214	−0.404	−0.424
	−0.379	−0.433	−0.455
	−0.410	−0.510	−0.510
	−0.771	−0.852	−0.852
	−0.997	−1.079	−1.083
H	0.681	0.268	0.268
	−0.266	−0.280	−0.280
	−0.266	−0.284	−0.290
	−0.266	−0.284	−0.290
	−0.908	−1.002	−1.034
	−0.954	−1.026	−1.040
P	0.372	0.346	0.333
	−0.367	−0.390	−0.404
	−0.367	−0.390	−0.404
	−0.700	−0.852	−0.855
	−0.700	−0.852	−0.855
	−0.814	−0.855	−0.863

In some qualitative sense, there is general agreement in the over-all shapes of the bands between various calculations for iron. Hence, it is not surprising that considerable similarity exists between the bands found here and those calculated by previous workers, particularly those whose methods allowed hybridization of s and d bands, such as Wood's[7] APW method and Wakoh and Yamashita's[8] Green's-function method. Although no analysis of the angular symmetry of the wave functions was performed for the present calculation, the striking resemblance of the bands to those of Wood implies that the allocation of the representations should be the same as his. Wakoh and Yamashita differ significantly at only one point: They connect one of the $\Gamma_{25'}$ states to N_1 and thence to the $H_{25'}$. Wood and the present calculation show the same state $\Gamma_{25'}$ to be connected to the $N_{1'}$ state and thence to the H_{12} state.

By making quantitative comparisons, significant differences between this calculation and those of other workers emerge. Table IV lists some relevant features. The most striking feature is the disparity in widths of the d bands. The following generalization appears to be valid: Those methods

TABLE IV. Comparison of some band-structure features of this calculation with those of other authors (Refs. 7 and 8). All energies are in Ry. GF = Green's function; APW = augmented plane waves; TB = tight binding; MTB = modified tight bindings; OPW = orthogonalized plane wave.

	This calculation	Wakoh and Yamashita[a] (GF)	Wood (APW)	Abate and Asdente (TB)	Ingals (MTB)	Stearn (MTB)	Callaway (OPW)
Splitting between doublet and triplet states							
At Γ majority spin	0.23	0.10	0.12	0.60	0.12	0.26	0.002
minority spin	0.18	0.11					
At H majority spin	0.75	0.35	0.44	0.76	0.44	0.59	0.070
minority spin	0.64	0.39					
At P majority spin	0.45	0.18	0.25	0.20		0.27	
minority spin	0.45	0.22					
Difference in energy between center of gravity of majority-spin d states and center of gravity of minority-spin d states							
At Γ	0.29	0.13					
At H	0.26	0.12					
At P	0.26	0.11					
Difference in energy between Γ_1 state and center of gravity of d states at Γ							
majority spin	0.67	0.44	0.58		0.51	0.164	
minority spin	0.87	0.53					
Spin splitting of Γ_1 states							
	0.10	0.034					
Over-all width of lowest six states at N							
majority spin	0.66	0.44	0.48	0.47[b]		0.68[b]	0.11[c]
minority spin	0.63	0.43					

[a]The results of De Cicco and Kitz are essentially identical to those of Wakoh and Yamashita.
[b]Since no s state was given, this is the spread of the lowest five states.
[c]The s state rises rapidly and no hybridization is included. This is, therefore, the spread of the lowest five states.

which explicitly utilize the overlap of d wave functions on different sites (the present work, Abate and Asdente, and Stern) tend to produce wider d bands than those methods which expand the wave functions in the interatomic region in terms of plane waves (Wakoh and Yamashita, De Cicco and Kitz, Wood, and Callaway). Even so, the present calculation produces wider bands than heretofore found. Noting that, here, the widths for majority-spin bands are greater than those for minority-spin bands, it is useful to try to separate out an exchange contribution to the bandwidth. Using Wakoh and Yamashita's estimation of the number of d electrons in each spin, we try to fit the splitting γ between the triplet and doublet states by expressions of the form

$$\alpha + \beta n_{\uparrow,\downarrow} = \gamma_{\uparrow,\downarrow} , \tag{38}$$

where α is the nonexchange contribution to the width, and β is the exchange contribution per spin. Using this, we find the contributions to the doublet-triplet splitting listed in Table V. Compared with these, the Green's-function method gives slightly wider minority-spin than majority-spin bands. The spin-independent parts found here agree with those from the Green's-function calculation. The very definite exchange contribution to width found here is directly related to the inclusion of two-center exchange matrix elements. Clearly, assumptions made about the effectiveness of exchange screening for d electrons by the s electrons or the limitation of the interatomic exchange by a localizing effect of correlation can have important consequences for the bandwidth.

Experimentally, photoelectric emission and reflectance studies[32,33] have suggested the presence of much wider d bands than had been predicted by

TABLE V. Analysis of doublet-triplet splitting at some symmetry points.

Symmetry point	Nonexchange contribution	Exchange contribution Majority spin	Minority spin
Γ	0.12	0.11	0.06
H	0.53	0.22	0.12
P	0.45	0	0

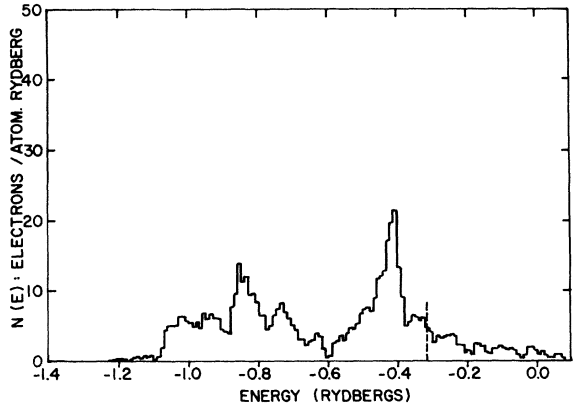

FIG. 5. Density-of-states histogram deduced for majority-spin electrons.

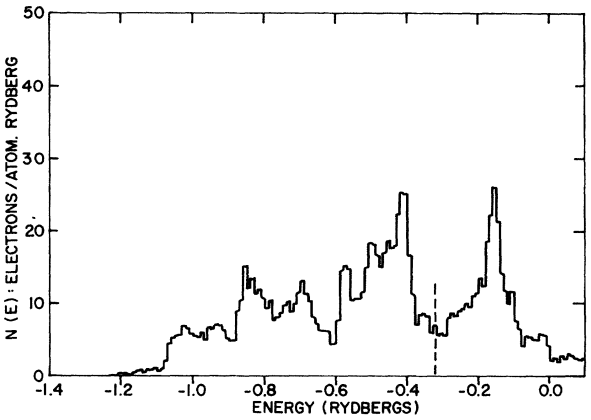

FIG. 7. Histogram of the total density of states.

previous theoretical band structures. Figures 5–7 depict, respectively, the density-of-states curves for majority spin, minority spin, and total electrons as found by the method described in Sec. VII. Peaks in the total density of states occur at about 0.19, 0.39, and 0.54 Ry below the Fermi level, and the occupied width of the d levels is about 0.8 Ry. The optical density of states as measured by Blodgett and Spicer[32] indicates three peaks, one of which is now attributed to surface contamination.[33] A second peak of small amplitude appears just under the Fermi surface and has no counterpart in the theoretical density of states presented here. The remaining experimental peak coincides with the total density-of-states maxima between -0.4 and -0.6 Ry. Eastman,[33] likewise, shows a peak of about this width in his experimental optical density of states, but his peak lies closer to the Fermi surface than the present theory depicts. However, some latitude exists for adjustment of the theoretical position of the Fermi energy, as discussed below.

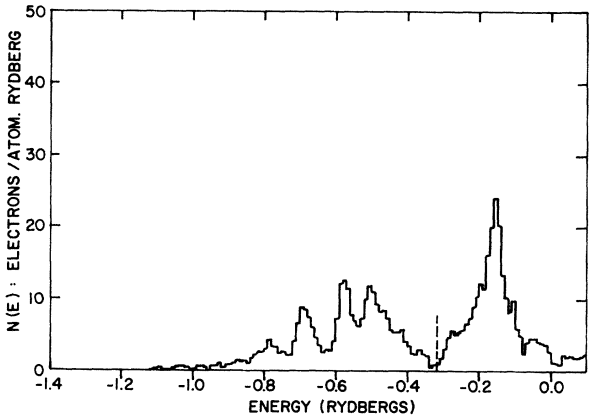

FIG. 6. Density-of-states histogram deduced for minority-spin electrons.

An examination of the x-ray emission spectra of iron also supports the picture of wide d bands. Figure 8 represents schematically the results of Tomboulian and Bedo[34] (their Fig. 5, M_3 emission band). They assumed the bandwidth to be given by the interval ED of Fig. 8, i.e., about 8 eV. If we accept at least part of the previously ignored spectra, the bandwidth could be as large as 11 eV (A D on Fig. 8). Moreover, if the kink at B is interpreted as a point of superposition of two curves, one for spin-up d electrons and the other for spin-down d electrons, the energy interval from A to B would give the magnetic splitting at the bottom of the d band of about 5 eV, in good agreement with our theoretical value of 4.5 eV at the point H, which also happens to be the point where the magnetic splitting is largest. Further experimental clarification of this is desirable.

VII. DENSITY OF STATES: FERMI ENERGY AND WORK FUNCTIONS

The density of states for each spin was found by the following method: Each of the 110 $\vec{k}$ vectors at which energies were calculated was considered to represent all points within a volume element al-

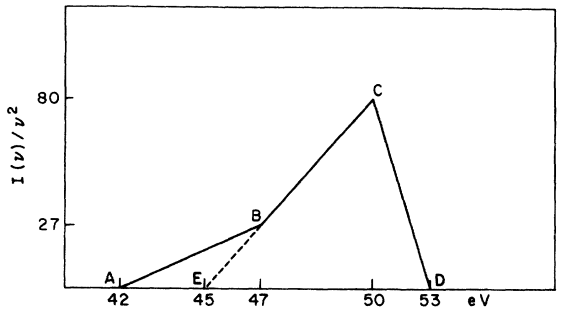

FIG. 8. Schematic representation of x-ray emission spectra given by Tomboulian and Bedo (Ref. 34).

located to and containing the $\vec{k}$ vector such that all of the volume elements filled the $\frac{1}{48}$ BZ. A number of equally spaced energies were chosen and each was compared with the energy of every state at every $\vec{k}$. For those states with lower energy than the test energy, a contribution equal to the associated volume element was added to a running total. Then the grand total was multiplied by 48 (BZ volume). This gave a numerically tabulated curve of total available states less than or equal to a given energy. The number of states available in a given energy interval is then simply the difference of the tabulated values at neighboring energy values.

The Fermi energy was found by adding the total available states curves for the two spin states and choosing that energy which contained eight electron states. The energy so found is -0.314 Ry.

It is to be noted that, unlike some methods of calculating band structures, the present method does not have inserted in it an arbitrary zero of energy. That is, Coulomb potentials were always treated with the potential of free space as the zero of energy. Thus, the value of the Fermi energy should have some absolute significance. In this case, the Fermi energy $= -0.314$ Ry $= -4.27$ eV is just a little less than the negative of the work function of 4.7–4.8 eV.[32] This should be regarded as good agreement, since the mechanism of photoemission is more than just the raising of the electron's energy by an amount equal to the difference between the Fermi energy and the potential of free space. There will certainly be some collective phenomena generated in the remaining electrons. Then, complicating the issue is the profound effect that surface dipole moments may have on the absolute value of the Fermi energy. In this context, it is relevant to point out that the method used in the present calculation to cancel the potential of the nuclear charges against the potential of the electron charges is tantamount to constructing a model for the surface; i.e., the crystal is a regular array of neutral cells, not only in the interior, but also at the surface. The good agreement between the work function and the Fermi energy may be interpreted to mean that the charge distribution near the surface does not differ greatly from the charge distribution in the interior, and only small electric polarization or dipole moments exist at the surface.

VIII. MAGNETIC MOMENT AND ORIGIN OF FERROMAGNETISM

In Secs. III and V the method of incorporating exchange and correlation in the band calculation was described. In particular, an effective one-center exchange contribution was calculated on the basis of a formula by Hubbard in which an assumption about the d bandwidth had to be made. Two band structures were calculated here, the first with the value $\Delta = 0.4$ Ry and the second with $\Delta = 0.55$ Ry. The second value of Δ seems more appropriate to the wider d bands found here than the smaller value. Of course, there exists the problem of the exact meaning of Δ. The over-all width from the bottom of the majority-spin band to the top of the minority-spin band does not seem to be a reasonable interpretation. Even the extremes of lowest energy to highest energy within a band of one spin may not be the best way to choose Δ, since these extremes may represent only a small proportion of states. It seems plausible to use $\Delta = 0.55$ Ry, which is approximately the distance between the two prominent peaks on each of the density-of-states curves in Figs. 5 and 6. In any case, we have no guarantee that the effective exchange formula is precise and, in fact, it is probably not precise, but it should give a good estimate of the correlation effects.

The magnetic moment is readily obtained by subtracting the total number of states under the Fermi energy for the minority-spin bands from the total number of states under the Fermi energy for the majority-spin bands. In this way the magnetic moment for $\Delta = 0.4$ Ry was 2.06 μ_B/atom and that for $\Delta = 0.55$ Ry was 2.19 μ_B/atom. Experimentally, the magnetic moment is 2.2 μ_B/atom. Thus the model has given, within the limitations involved in assuming Hubbard's formula, a first-principles derivation of the magnetic moment.

To explore the role of correlation further, the bandwidth Δ was regarded as an adjustable parameter and the corresponding values of the effective exchange calculated. Using this to produce a rigid-band shift of the spin states relative to one another, an approximate estimate of the dependence of the magnetic moment on Δ is found. The solid curve of Fig. 9 is the magnetic moment which results from given rigid-band displacements, and the dotted curve graphs the rigid-band shift as a function of Δ. The magnetic moment is characterized by a steep rise to about 2.18 μ_B/atom and then a broad plateau to 2.25 μ_B/atom followed by another steep rise. The plateau is produced when both spin states have minima of their density of states at the Fermi surface, and conversely the steep sections are characterized by a maximum of the density of states of either spin (or maxima for both spins) at the Fermi surface. The experimental value of the magnetic moment is equal to the plateau value and thus corresponds to the saturation of the prominent peak in the density-of-states histogram. Over the plateau region very large changes in Δ produce only minor changes in the magnetic moment, so in this range the choice of Δ or the accuracy of Hubbard's formula is not critical. However, its dominant role in producing the ferromagnetic moment is

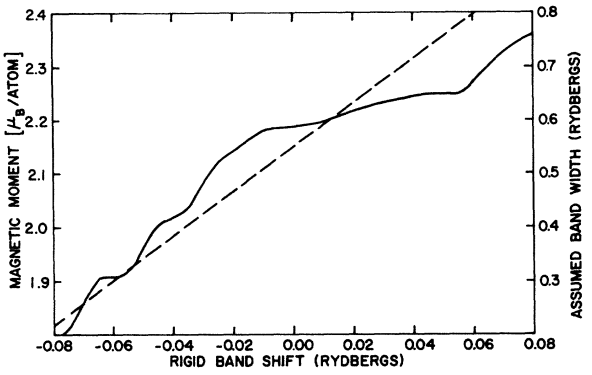

FIG. 9. The solid line is a graph of the magnetic moment which would result from a rigid-band shift of the minority-spin states with respect to the majority spin. The dashed line gives the rigid-band shift resulting from Hubbard's formula [Eq. (36)] as a function of the assumed bandwidth.

revealed by the rapid decrease in moment for Δ less than about 0.5 Ry. For $\Delta = 0$, the magnetic moment would be 1.3 μ_B/atom, implying that the remaining 0.9 μ_B/atom comes from itinerancy of the d electrons. For large Δ corresponding to increased itinerancy, the magnetic-moment curve increases steeply, and finally represents minority d states completely above all majority d states.

It is interesting to speculate on the outcome of an attempt to iterate to self-consistency the band with an assumed $V_{eff} = 0$ corresponding to $\Delta = 0$. For a start we would have to inject a polarization of 1.3 μ_B/atom instead of 2.2 μ_B/atom, and the resulting band magnetic moment would certainly be lower than 1.3 μ_B/atom. It is possible that the magnetic moment would sink to zero and the iron would be paramagnetic. If this happened, it would indicate that the role of the itinerant contribution to the magnetic moment has decisive importance. In fact, without this contribution there is little physical mechanism for the spin at one site to become coupled to that on another site.

The following mechanism for the origin of iron's ferromagnetism is therefore suggested. Hund's rule at a given site is initially responsible for polarizing the electrons at that site. This is amplified by some itinerant ferromagnetism of the d states, and the itinerancy of the d electrons couples the moments on the different sites. Without the itinerancy, iron would not be ferromagnetic. The formula given by Hubbard, while being partially qualitative, appears quantitatively useful for practical computations based on this model. It will be argued in a subsequent paper[6] that the indirect coupling through the s states produced by the RKKY mechanism actually opposes the tendency to ferromagnetism.

Figure 9 shows that there is some flexibility for arbitrarily shifting the two density-of-states curves, without altering the magnetic moment appreciably. This means that the total density of states at the Fermi surface can be adjusted over a wide range, from a small value ($\approx$ 5–10 electrons/atom Ry) on the plateau to a large value ($\approx$ 20–40 electrons/atom Ry) on the steep section, without significantly changing the magnetic moment. The corresponding range of theoretical specific heats is $2\text{–}16\times10^{-4}$ cal/mole °K, where the experimental value[35] is 12×10^{-4} cal/mole °K. Because it is possible to vary the theoretical density of states at the Fermi surface so widely, it is not possible to use the electronic specific heat or susceptibility as a gauge of the merit of the band structure of this ferromagnetic metal.

IX. FERMI SURFACE

No attempt has been made here to depict a Fermi surface; however, it is possible to comment on one minor point. Because their $N_{1'}$ representation for the majority-spin band is well above the Fermi level, Wakoh and Yamashita[8] find tubular arms to the Fermi surface surrounding the HNH line. This implies the existence of a closed de Haas–van Alphen orbit of small area equal to the tube's maximum cross-sectional area, but there has been no experimental verification of the existence of this orbit.[36] The cause of the $N_{1'}$ state being so energetic is the proximity of the d bands to the s bands. In the present calculation, the Γ_1 level lies further below the d bands and so, if the tubes exist at all around H or around any part of the HN line, they are pinched off before they reach N. The nonexistence of the orbit in question is then very indirect evidence that the s bands are further below the d bands than Wakoh and Yamashita have depicted them. The relative depth of the Γ_1 point has been considerably affected by the Coulomb-hole contribution.

Recently Fivaz[37] has attempted to explain an anomalous behavior of the spontaneous Hall effect reported by Dheer[38] on the basis of an assumed degeneracy of the levels Δ_2 and Δ_5 in the minority-spin bands at the Fermi energy. In the present calculation, the Δ_2 and $\Delta_{2'}$ bands of the minority spin cross at the Fermi level, but these do not explain the anomaly because a second criterion, namely, the existence of a nonzero spin-orbit matrix element between the otherwise degenerate states, is not met by these two states.

X. CONCLUSION

In this paper we report a new band-structure calculation for the ferromagnetic state of iron, in which exchange and correlation effects have been given a detailed treatment. Because of the inclusion of two-center exchange integrals, the bands

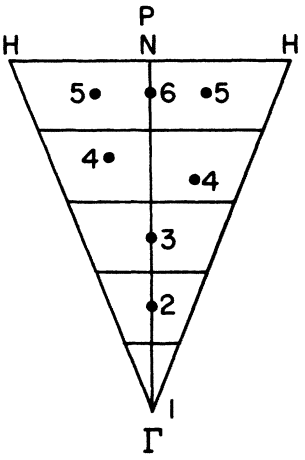

FIG. 10. Positions of the sample points used in the calculation of matrix elements illustrated for $\frac{1}{12}$ BZ.

found here are wider than those published before. Some support for the idea of wider bands has been found in optical and x-ray experiments. The calculation has verified the description of the band electrons as being intermediate between fully localized and fully itinerant by demonstrating the feasibility of calculating the magnetic moment in an almost first-principles fashion. The calculated Fermi energy is close to the negative of the work function.

ACKNOWLEDGMENTS

We are grateful for the cooperation and assistance given to us by Dr. M. Garber, Director of the Computing Center, University of California, Riverside. Dr. T. Gilbert of Argonne National Laboratory kindly supplied us with the wave functions for the $3d^7 4s$ configuration, and this is gratefully acknowledged. One of us (K. J. D.) thanks the Phi Beta Kappa Alumni in Southern California for financial support via an International Student Scholarship.

APPENDIX: SELECTION OF SAMPLE STATES

It is clear that the BZ (Fig. 2) can be divided into 12 pyramids, each with a diamond-shaped base with corners *PHPH* and apex Γ. The midpoint of the *HH* line or *PP* line is *N*. Take the Γ*N* line as the *Z* axis and the length $\Gamma N = Z_0$. Let the *HH* line be the *X* axis of length $HH = X_0$; the *PP* line is the *Y* axis of length Y_0. Then the sample points are as depicted in Fig. 10 and listed below:

Point	Coordinates
1	0, 0, 0
2	$0, 0, \frac{3}{10} Z_0$
3	$0, 0, \frac{5}{10} Z_0$
4	$\frac{7}{80}X_0, \frac{7}{80}Y_0, \frac{7}{10} Z_0$
	$-\frac{7}{80} X_0, -\frac{7}{80} Y_0, \frac{7}{10} Z_0$
5	$\frac{9}{40} X_0, 0, \frac{9}{10} Z_0$
	$-\frac{9}{40}X_0, 0, \frac{9}{10} Z_0$
6	$0, \frac{9}{40} Y_0, \frac{9}{10} Z_0$
	$0, -\frac{9}{40} Y_0, \frac{9}{10} Z_0$

These points are repeated in each of the 12 pyraminds, making a total of 97 sample points.

---

*Present address: Scientific Research Staff, Ford Motor Company, P.O. Box 2053, Dearborn, Mich. 48121.

†Present address: Physics Department, University of Utah, Salt Lake City, Utah 84112.

[1]See, for example, J. Calloway, *Energy Band Theory* (Academic, New York, 1964), and references quoted therein.

[2]P. W. Anderson and A. M. Clogston, Bull. Am. Phys. Soc. 6, 124 (1961); N. F. Mott, Advan. Phys. 13, 325 (1964).

[3]L. Hedin, Phys. Rev. 139, A796 (1965); Arkiv. Fysik. 30, 231 (1965).

[4]J. Hubbard, Proc. Roy. Soc. (London) A276, 238 (1963); A277, 237 (1963); A281, 401 (1964).

[5]L. Hodges, H. Ehrenreich, and N. D. Lang, Phys. Rev. 152, 505 (1966).

[6]K. J. Duff and T. P. Das (unpublished).

[7]M. F. Manning, Phys. Rev. 63, 190 (1943); J. Callaway, *ibid.* 99, 500 (1955); E. F. Belding, Phil Mag. 4, 1145 (1959); F. Stern, Phys. Rev. 116, 1399 (1959); M. Suffczynski, Acta. Phys. Polon. 20, 945 (1961); J. H. Wood, Phys. Rev. 126, 517 (1962); L. F. Mattheiss, *ibid.* 134, A970 (1964); E. Abate and M. Asdente, *ibid.* 140, A1303 (1965); R. Ingalls, *ibid.* 155, 157 (1967); J. Hubbard and N. W. Dalton, J. Phys. C 1, 1637 (1968).

[8]S. Wakoh and J. Yamashita, J. Phys. Soc. Japan 21, 1712 (1966).

[9]P. De Cicco and A. Kitz, MIT Solid State and Molecular Theory Group Quarterly Progress Report No. 62, 1966, p. 13; 63, 1967, p. 2 (unpublished).

[10]P. D. De Cicco and A. Kitz, Phys. Rev. 162, 486 (1967).

[11]J. W. D. Connolly, Intern. J. Quantum Chem. 2, S257 (1968).

[12]B. W. Batterman, D. R. Chipman, and J. J. DeMarco, Phys. Rev. 122, 68 (1961).

[13]C. G. Shull and H. A. Mook, Phys. Rev. Letters 16, 184 (1966).

[14]C. J. Shull and Y. Yamada, J. Phys. Soc. Japan Suppl. 17, 1 (1962); C. G. Shull, Verband Deutscher Physikalischer Gesellschaften. Physikertagung. Hauptvortrage, 1962 (unpublished).

[15]P. E. Mijnarends and L. Hambro, Phys. Letters 10, 272 (1964).

[16]D. H. Anderson, Solid State Commun. 4, 189 (1966).

[17]*A posteriori* we disagree with the interpretation of the

experimental evidence. This calculation yields a positive s-band polarization; a full discussion is given in Ref. 6.

[18]E. Clementi, IBM J. Res. Develop. 9, 2 (1965).

[19]T. Gilbert (private communication).

[20]David Pines, *The Many Body Problem* (Benjamin, New York, 1952).

[21]R. R. Sharma, J. Math. Phys. 9, 505 (1968); K. J. Duff, Intern. J. Quantum Chem. (to be published).

[22]P. O. Löwdin, Advan. Phys. 5, 1 (1956).

[23]M. E. Rose, *Elementary Theory of Angular Momentum* (Wiley, New York, 1957).

[24]J. C. Phillips and L. Kleinman, Phys. Rev. 128, 2098 (1963).

[25]J. C. Phillips, Phys. Rev. 123, 420 (1961).

[26]William Brinkman and Bernard Goodman, Phys. Rev. 149, 597 (1966).

[27]G. D. Gaspari, Ph.D. dissertation, University of California, Riverside, 1964 (unpublished).

[28]S. D. Mahanti, Ph.D. dissertation, University of California, Riverside, 1968 (unpublished).

[29]J. Kanamori, Progr. Theoret. Phys. (Kyoto) 30, 275 (1963).

[30]M. C. Gutzwiller, Phys. Rev. 134, A923 (1964).

[31]A review of the experimental evidence supporting this is given by C. Herring, in *Magnetism*, edited by G. T. Rado and H. Suhl (Academic, New York, 1966), Vol. IV.

[32]A. J. Blodgett and W. E. Spicer, Phys. Rev. 158, 514 (1967).

[33]D. E. Eastman, J. Appl. Phys. 40, 1387 (1969).

[34]D. H. Tomboulian and D. E. Bedo, Phys. Rev. 121, 146 (1961).

[35]M. Horowitz and J. G. Daunt, Phys. Rev. 91, 1099 (1953).

[36]A. V. Gold, J. Appl. Phys. 39, 768 (1968).

[37]R. C. Fivaz, J. Appl. Phys. 39, 1278 (1968).

[38]P. N. Dheer, Phys. Rev. 156, 637 (1967).

PHYSICAL REVIEW B VOLUME 3, NUMBER 1 1 JANUARY 1971

Exciton-Exciton Transitions in MnF_2

S. E. Stokowski and D. D. Sell
Bell Telephone Laboratories, Murray Hill, New Jersey 07974
(Received 27 August 1970)

Transitions involving the simultaneous creation of two excitons in MnF_2 are reported. These double excitons are combinations of the $E1$(18 419.6 cm^{-1}) and $E2$ (18 436.6 cm^{-1}) single excitons. Line transition identified as $E2+E2$ (36 789 cm^{-1}) and $E1+E2$ (36 917 cm^{-1}) were seen; however, the transition to the $E1+E1$ state was not observed. The identification was made with the aid of uniaxial stress measurements; the energy shifts of the double excitons under stress are simply related to those of the $E1$ and $E2$ excitons. It is shown on the basis of one-electron molecular orbitals that for the $E1+E1$ state the exchange interaction, and thus the transition probability, is small. The observed polarization of the double exciton lines is explained in terms of the Mn pair symmetry. It has also been confirmed that the $E1$ exciton transforms as the B_3 representation of the group D_{2h}.

I. INTRODUCTION

The study of antiferromagnetic insulators in recent years has led to the observation of double excitations, such as magnon-magnon,[1,2] exciton-magnon,[3,4] and exciton-exciton[5,6] transitions. These two-center excitations provide information about the magnon dispersion and density of states, molecular fields, and the exchange interaction between magnetic ions. In this paper we present and discuss the observation of double-exciton transitions in MnF_2. These transitions are the result of the absorption of a photon and the creation of two excitons in the lowest-energy $^4T_1$ state of the Mn^{2+} ion.

Exciton and exciton-magnon absorption were first seen in MnF_2 by Greene *et al.*[3] They observed exciton transitions, which they labeled $E1$ (18 419.6 cm^{-1}) and $E2$ (18 436.6 cm^{-1}), between the $^6A_1$ ground state and two states of the $^4T_1$ manifold of Mn^{2+}. Dietz, Misetich, and Guggenheim[7] found, through uniaxial pressure experiments, that $E1$ and $E2$ could be characterized by linear combinations of the $(\pm 1, \frac{3}{2})$ components of the $^4T_1$ state. Because these two states are only 17 cm^{-1} apart, the effective spin-orbit parameter for the $^4T_1$ state must be small. Some calculations have been done on the energy splittings of the $^4T_1$ states, but with only limited success in explaining the experimentally observed splittings. Both Meltzer and Lohr[8] and Washimiya and Gondaira[9] suggested that the smallness of the spin-orbit coupling is due to vibronic interaction. Exciton-magnon fluorescence has been studied by Dietz and Misetich.[10] Their results indicate that the $E1$ and $E2$ excitons have no measurable dispersion, although later Dietz *et al.*[11] found a thermodynamic distinction between the zone-center and zone-boundary exciton states. Thus, for most purposes, the excitation can be considered as being localized on a particular ion.

Previously, exciton-exciton transitions were